Journal of Flood Risk Management

WILEY | CIWEM Chartered Institution of Water and Environmental Management

ORIGINAL ARTICLE OPEN ACCESS

Geospatial Analysis of Population Exposure to Flooding in the Sudd Region, South Sudan

Deng Majok Chol[1] | Jim W. Hall[1] | Kevin G. Wheeler[2,3] | Mark Bernhofen[4] | Courtney A. Di Vittorio[5] | Kenneth M. Strzepek[6]

[1]Oxford Programme for Sustainable Infrastructure Systems, Environmental Change Institute, School of Geography and the Environment, University of Oxford, Oxford, UK | [2]Environment Change Institute, Oxford, UK | [3]Water Balance Consulting, Boulder, Colorado, USA | [4]Environmental Change Institute, School of Geography and the Environment, University of Oxford, Oxford, UK | [5]Department of Engineering, Wake Forest University, Winston-Salem, North Carolina, USA | [6]MIT Center for Sustainability Science and Strategy, Cambridge, Massachusetts, USA

Correspondence: Deng Majok Chol (deng.chol@ouce.ox.ac.uk; dengmchol@yahoo.com)

Received: 24 April 2025 | **Revised:** 4 November 2025 | **Accepted:** 17 December 2025

Keywords: flood hazards | model intercomparison | population exposure | South Sudan | Sudd region

ABSTRACT

The Sudd wetland in South Sudan extends over 90,000 km^2. Large-scale flood events in recent years (2019–2022) are said to have led to the displacement of an estimated 1.8 million people in total. However, these estimates are approximate and to date there has not been a systematic analysis of population exposure to flooding in the Sudd region. This study seeks to address this gap by using global flood modeling, satellite observations of flood extent, and global gridded population datasets to analyze population exposure. Recognizing the inevitable limitations of these datasets, we intersect all the available global flood mapping and population datasets. The results indicate that 0.8–2.9 million people are currently exposed to the 100-year return period flood extent, depending on the flood model and population dataset used. Aggregated results of the model agreement intercomparison indicate that all five global models agree on key flood-prone areas within and around the Sudd, which is further corroborated with satellite flood observations. Intercomparison of the population density among the four georeferenced population products demonstrates that WorldPop and GHSL-Pop population distributions better represent the patterns of the Sudd rural settlements that are typically in forms of clusters. The uncertainty in exposure estimates is attributable to variations in both flood outlines and geospatial population estimates. These findings provide hitherto unavailable insights into flood exposure in South Sudan, to inform flood management decisions and disaster reduction responses in the Sudd region. This study demonstrates the global significance of model intercomparison as best practice for any flood exposure analysis to underpin policy and decision-making in Africa and other data-scarce regions.

1 | Introduction

Whilst more than a billion people across the world depend on wetlands for their livelihoods (United Nations 2023), population exposure to flood hazards around wetlands and within floodplains has been increasing rapidly (Andreadis et al. 2022; Rentschler et al. 2022, 2023; Jongman et al. 2012). Though global exposure to flood risk is increasingly studied (McMichael et al. 2020; Hirabayashi et al. 2021; Bernhofen et al. 2021; Jongman et al. 2012), the exposure of populations inhabiting or neighboring wetlands has proved to be difficult to quantify. This reflects the difficulty of flood modeling in complex, low-lying, and highly vegetated landscapes (Trigg et al. 2016) and may also reflect the low wealth of wetland populations, which means that they have not been a priority for flood modeling by the insurance sector. In low-income regions of the world such as South Sudan where water infrastructures are limited or non-existent, flooding is a key threat facing communities. This study focuses on

the Sudd, a term derived from the Arabic word, sadd (سد) which means barrier or obstruction. In the Sudd region, local communities have always had to cope with flooding and have adopted practices that benefit from the proximity to water (e.g., for livestock watering) whilst seeking to inhabit less exposed locations. However, geomorphological processes, poverty, changing cultural practices (e.g., swift shifts from nomadic lifestyles to more fixed habitations), and the disruption of the development of the social and economic fabric of the societies through successive wars (1983–2005; 2013–2018) exacerbate communities' exposure and vulnerability to flooding. The dramatic flood events of the past 4 years (2019–2022) have manifested total displacement of an estimated 1.8 million people (Internal displacement Monitoring Centre 2023) in the Sudd region.

Given the changing complex hydrology, limited hydrological observations, and weak local expertise due to decades of conflict, there is no large-scale local modeling of flooding processes in the Sudd region. This paper therefore makes use of global flood modeling outputs, comparing them with one another, with gauged data and with satellite flood observations to evaluate their accuracy. These flood model predictions are intersected with a range of recently released global georeferenced population products to estimate the population exposed to flooding in and around the perimeter of the floodplains of the Sudd. The results from this study demonstrate the global significance of model intercomparison as best practice for any flood exposure analysis to underpin policy and decision-making in Africa and other data-scarce regions.

2 | Study Area

2.1 | Hydrology

The Sudd is the largest tropical wetland in the world, covering a vast area of approximately 57,000–90,000 km^2 (Nile Basin Initiative 2020) and situated in South Sudan in the lower reaches of Bahr el Jebel/White Nile at an elevation of 380–450 m above mean sea level. All streamflow from the upper catchments, including mountain spring water in the African Great Lakes region and western highland of Ethiopia, drains into the Sudd (Figure 1), thereby enabling the thriving aquatic ecosystem and supporting the largest mammal migration in the world (African Parks 2024). The "Spade-like-Shape" of South Sudan, with a depression in the center of the country, is an accumulation conveyor for flood waters, making the Sudd a key part of the Nile River system that maintains steady flow year round.

The Sudd ecosystem services provide millions of people with livelihoods but also cause flooding in the Sudd region. The outflow from the equatorial lakes leads to strong seasonal inundation, characterized by annual flood pulses (Rebelo et al. 2012), which is further modified by local precipitation and evaporation (Mohamed and Savenije 2014), leading to highly complex and seasonal behavior (Sosnowski et al. 2016). The wetland area is a shallow depression, sloping gently to the north with a gradient of 1.0–1.5 cm/km (Nile Basin Initiative 2020). The Sudd extent varies from season to season, inter-annually, and over decades. Due to increased rainfall in the African Great Lakes region from 1961 to 1964, severe flooding occurred in the Sudd region and the Sudd extent increased by 300% (Nile Basin Initiative 2020; Gowdy and Lang 2016). However, from 1965 to 1978, the Sudd extent decreased by 47% due to prolonged drought (Lamberts 2009).

Previous researchers have adopted different boundaries for the study of the Sudd wetland. These sizes range from relatively small areas of 8000 km^2 to large areas of 100,000 km^2. These varying estimates of the Sudd extent demonstrate high levels of intra- and inter-annual hydrological variability and the overall lack of standardized and long-term monitoring data on the extent of water bodies. This can be increasingly addressed through satellite products (Borgomeo et al. 2023; Persico et al. 2024) that provide wide spatial coverage, near real-time data acquisition, ability to monitor remote areas, penetration through cloud cover and detailed mapping of flood extent. The consensus for the Sudd extent is in the range 57,000–90,000 km^2, which is supported by several literature sources (Figure 2) including UNESCO's designation of an area of 57,000 km^2 of the Sudd as a Ramsar Wetland (UNESCO World Heritage Convention 2006). However, this range in the Sudd extent is surpassed during extreme flooding such as in the 1960–1964 and 2019–2022 flood events.

Some of the previous works (Figure 2) including Balek (1977), Mohamed and Savenije (2014), Tootchi et al. (2019), and UNEP (2018) have not specified measurement methods that were used to determine the size of the Sudd. However, several other authors (Figure 2) have used various measurement methods to derive the Sudd sizes. These methods include water balance and aerial surveys (Hurst and Phillips 1938), remote sensing (Mason et al. 1992), surveys, remote sensing (Travaglia et al. 1995), water balance model (Sutcliffe and Parks 1999), remote sensing (Mohamed et al. 2004), regional climate model (Mohamed et al. 2005), and remote sensing (Di Vittorio and Georgakakos 2021).

Evapotranspiration exceeds precipitation during 9 months of the annual cycle, hence direct rainfall over the Sudd is a minor contributor to the water balance of the Sudd (Mohamed and Savenije 2014). The Sudd wetland (Figure 1) hydrology and water balance are mainly influenced by precipitation variations upstream of the Sudd and changing water levels of Lakes Victoria, Kyoga, George, Edward, and Albert (Mohamed and Savenije 2014; Mahgoub Mohamed 2021; Howell 1983; Howell et al. 1988; Sutcliffe and Parks 1999). An estimated 75% of inflow water originates from the equatorial lakes and 25% comes from torrents between Lake Albert and Mongalla (Mohamed and Savenije 2014; Birkett et al. 1999; Nicholson 2017; Nicholson and Yin 2001).

Historical accounts (Figure 3) report five major floods in some parts of the Sudd region in the nineteenth century: 1820–5, 1878, 1894, 1895, and 1896 floods. The 1820s flood lasted about 5 years, resulting in significant deaths, destruction of livelihoods, and long-term displacement and migration of the communities (Johnson 1992, 2019). In the twentieth century, communities in the Sudd region were devastated by major floods in 1916–17, 1931, 1932, 1944, 1961–64, 1989–91, and 1991 (Johnson 1992). These past extreme flood events reportedly caused destruction of properties and human suffering. Lately, floods of this magnitude devastated South Sudan in 2019–2022, inundating four

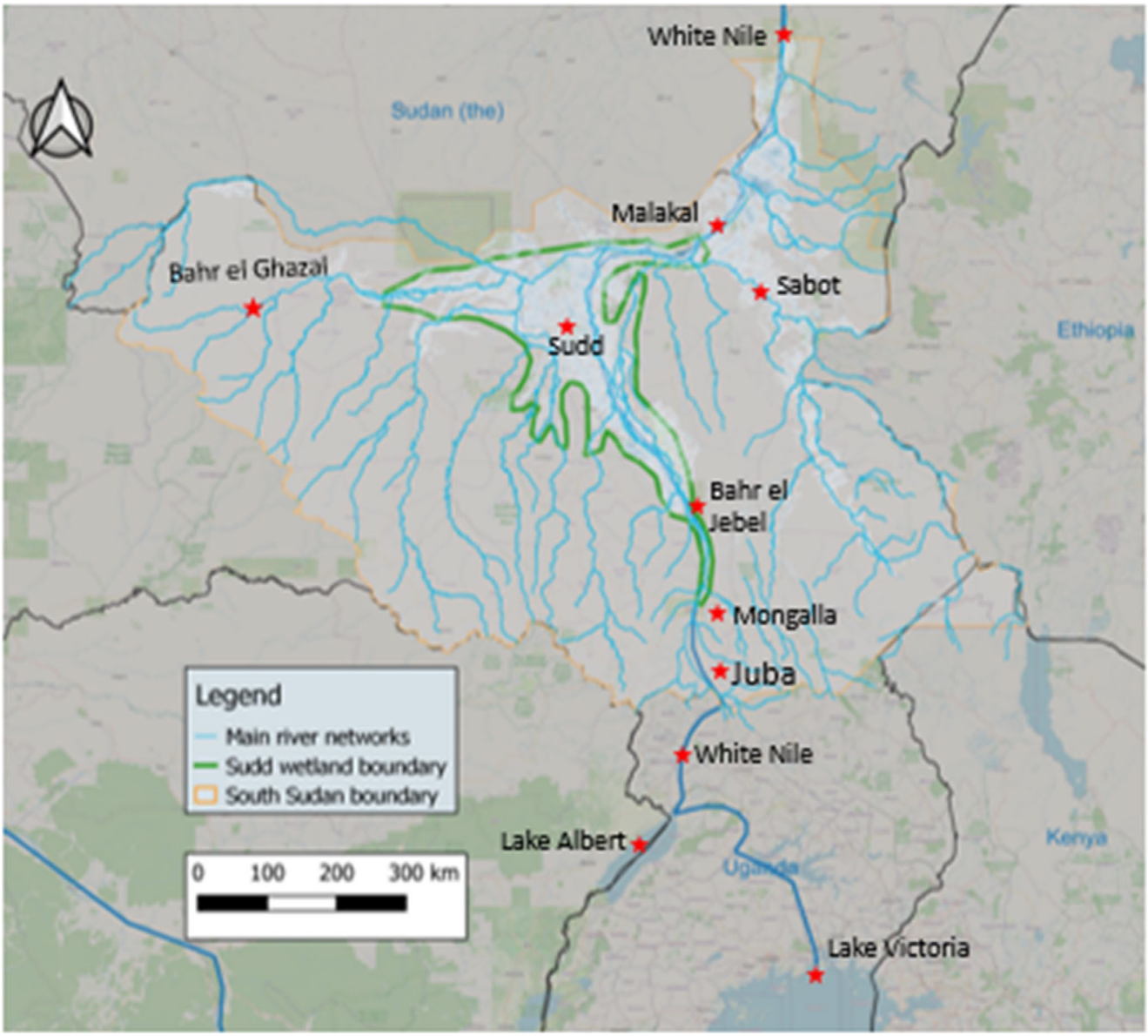

FIGURE 1 | The Sudd region study. The figure depicts the White Nile from the equatorial lakes region and through South Sudan; the Bahr el Jebel basin; the Sudd entrance at Mongalla; the Sudd exit at Malakal; the Bahr el Ghazal basin; and the Sobat basin.

of the ten states that are predominantly in the Sudd region floodplains.

Those major flooding events caused highly disruptive impacts to former Bor-Duk District (now, Duk county, Twic East County, and Bor County) in Jonglei State, major parts of Ayod, Old Fangak and Nyirol counties in Jonglei State, and Khor Atar (now, a county) in Jonglei State.

During the period of 1905–1983, discharge peaks from the equatorial lakes of over 30 billion m^3/year (Figure 3) at Mongalla (Figure 1) tends to be associated with flood occurrence reports in the Sudd region. This linkage is further evidenced by stream inflow and runoff increases during 2019–2022 that raised the water level in Lake Victoria by 13.42 m above sea level in May 2020, surpassing the 13.41-m, the previous highest recorded water mark in 1964 (Lake Victoria Basin Commission 2020). The resultant substantial inflow into the Sudd caused dramatic flooding in South Sudan during the same period. The cumulative impacts of these flood events include population displacement, ecosystem degradation, and inter-communal conflicts over access to a few dry islands within the Sudd and limited water and environmental resources.

2.2 | People and Population

The Sudd supports different ethnic groups who temporarily migrate during the wet-dry interseason to make use of the services the Sudd ecosystem provides (Rebelo et al. 2012). Gowdy and Lang (2016) found most of the local people of the Sudd region are Nilotic-speaking people (Dinka, Nuer, Shilluk, Luwo, Mundari, Jale, Maban, Anuak, and Murle) who are agro-pastoralists (Howell 1983; Howell et al. 1988; Evans-Pritchard 1940) that have adapted their economies and cultures to the demands of the hydrological cycles of the Nile. These nomadic

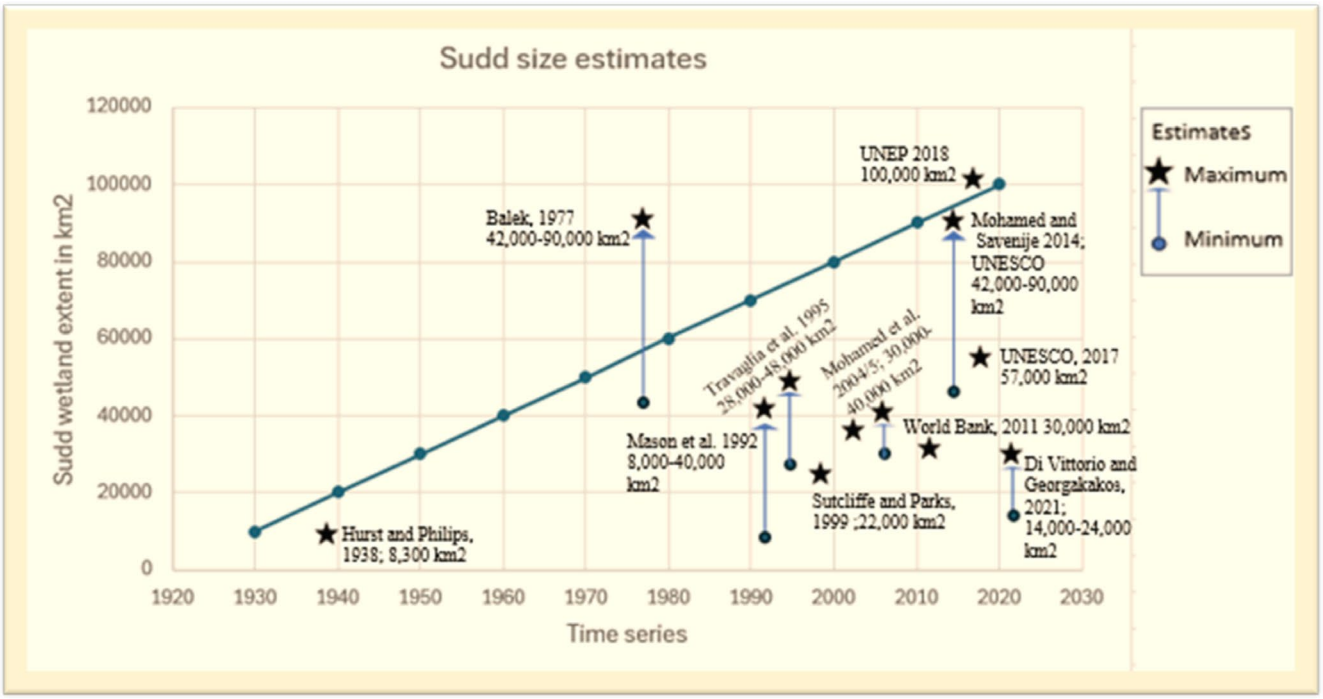

FIGURE 2 | The Sudd wetland: Varying estimates of the size of the Sudd extent.

local communities rely on the seasonal flooding to recharge soil moisture and regenerate the grasslands that support their cattle, their primary source of food and income (Howell et al. 1988; Di Vittorio and Georgakakos 2021). Most of the local populations move from their permanent settlements on the highlands to grazing in the intermediate lands (toich/swamps) at the beginning of the dry season and return to the highlands in May–June when the rainy season starts (Gowdy and Lang 2016). The wetland flooding regime has defined the livelihoods of millions of people who live in the Sudd region.

South Sudan's population estimates are uncertain. The country has not conducted a population and housing census since its independence from Sudan in 2011. As it was an autonomous region within Sudan, South Sudan's last population and housing census was conducted in 2008 as part of the 2005 Comprehensive Peace Agreement (CPA) that ended the 21-year long war between the Southern Sudan region (now South Sudan) and the Government of Sudan. (See Supporting Information for analysis of challenges of population counts in South Sudan.) In all these works, no specific population estimate was provided for the Sudd wetland region, but UNESCO World Heritage Centre (2017) estimated that one million people inhabit the Sudd wetland region. This estimate is low compared to extrapolations of population based on estimates from the 2008 Census for the states or counties that are predominantly in the Sudd region, which would suggest three to five million people currently reside in the Sudd region. These discrepancies justify a more comprehensive assessment of the affected population in this vulnerable region.

3 | Data and Methods

We used five global data sets of flood hazard, four global data sets of human population, satellite-derived earth observation inundation extent, and gauged discharge into the Sudd at Mongalla to analyze flood hazards and population exposure in the Sudd region. Flood exposures were calculated primarily for the permanent and seasonally flooded Sudd, including the western and eastern floodplains of the Sudd wetland. Flood exposures were also calculated for South Sudan at the national level, state level, and administrative areas. Principally, the states of Unity, Jonglei, Upper Nile, and Lakes as well as parts of Central Equatoria, Eastern Equatoria, Western Equatoria, and Warrap fall in the Sudd region.

3.1 | Global Flood Hazard Data

The Global Flood Models (GFMs) compared in this study are summarized in Table 1. The flood maps associated with the GFMs are typically presented with flood extent and/or depth at a given return period across the modeled domain (Bernhofen et al. 2022). These models were chosen because they were the only available models that provided hazard maps—at the time of research—in data-poor region of South Sudan. The outputs of the native flood hazard map of each GFM were acquired between January and July 2023. The outputs from Aqueduct, JRC, and CIMA-UNEP were obtained from open access databases. Respective developers provided the Fathom Global and CaMa-UT flood maps. Previous researchers including Bernhofen et al. (2022) compared these products in five countries at national scale; Trigg et al. (2016) assessed credibility of these products for African fluvial flood risks analysis; and Aerts et al. (2020) compared these products for flood hazard and exposed GDP in China as a case study.

The GFMs use different Digital Elevation Models (DEMs). FATHOM and CaMa-Flood v4 both use the Multi-Error-Removed Improved-Terrain DEM (MERIT DEM), which is a

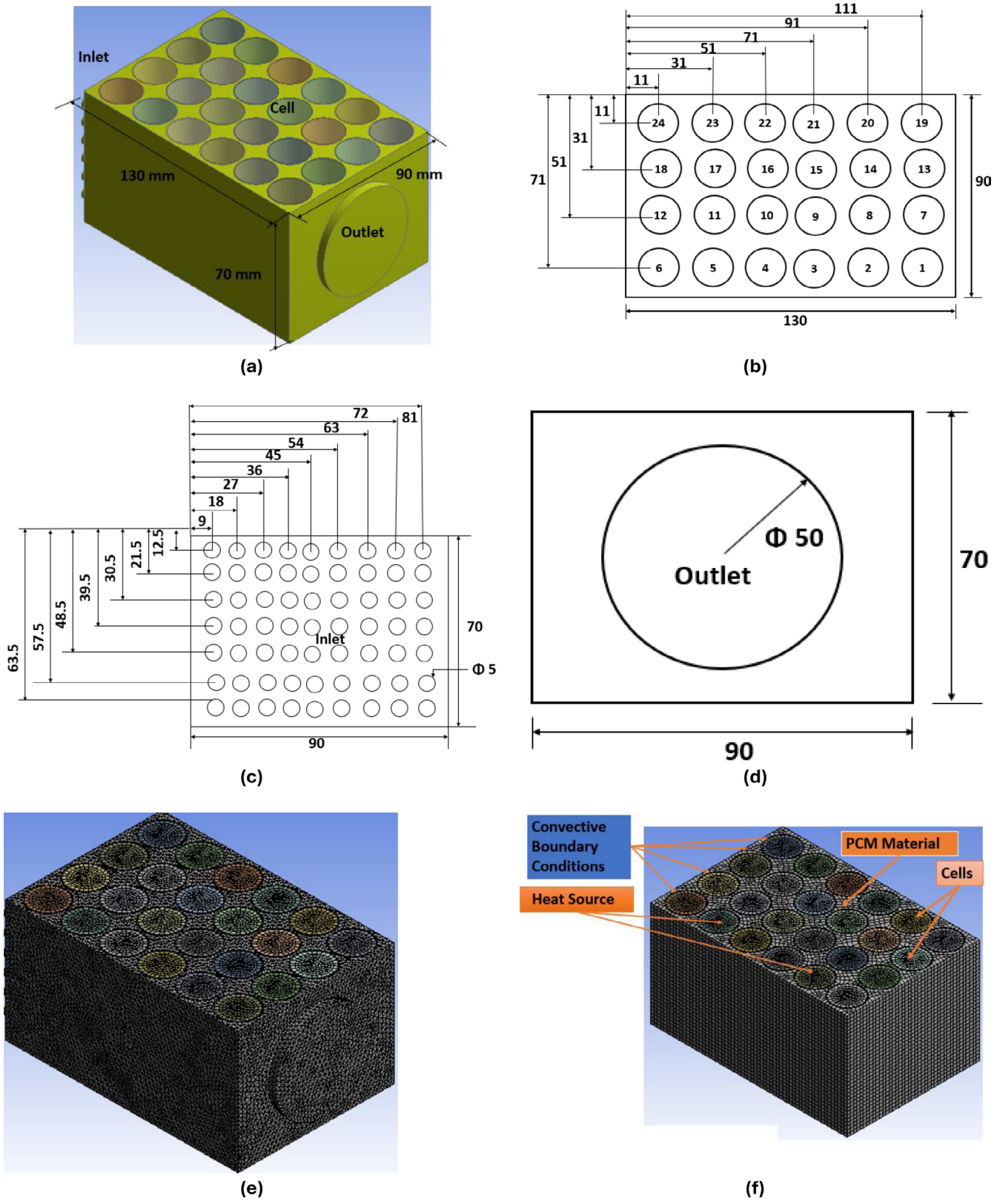

FIGURE 3 | The Sudd major flood timeline. This figure depicts years in which major flood events were reported (Johnson 1992) and gauged Nile flow (orange graphic line) from the equatorial lakes into the Sudd at Mongalla station (Egypt Nile Control Department 1933).

significant improvement as it "separates absolute bias, stripe noise, speckle noise and tree height bias using multiple satellite data sets and filtering techniques" to improve on the SRTM baseline (Yamazaki et al. 2017; Hirabayashi et al. 2021).

There are two different modeling approaches, the cascade model structure (CaMa-UT, GLOFRIS, and JRC) and the gauged-flow model structure (Fathom and CIMA-UNEP) (Trigg et al. 2016; Aerts et al. 2020). A detailed description of

TABLE 1 | Global flood models (GFMs) used in this study (adapted from Trigg et al. (2016)).

Model description	JRC global	GLOFRIS Aqueduct	CIMA-UNEP GAR 2015	Fathom 2.0 global	CaMa-UT 4.04
Model type	Cascade	Cascade	Gauged flow	Gauged flow	Cascade
Global climate dataset/global gauge dataset	ERA-Interim climate forcing dataset from 1980 to 2013	EU-WATCH global climate forcing dataset from ERA-40 reanalysis dataset, 1980–2015	EC-Earth and GRDC Global dataset of river discharge, 9500 stations record from 1960 to 2012, and 1981 to 2012	GRDC and USGS Global dataset of river discharge 9500 stations; record from 1983 to 2002 and 1807 to 2009	JRA-25 global climate forcing reanalysis dataset from 1979 to 2010
Land surface model	HTESSEL Global Hydrological Model (GHM)	The PCR-GLOBWB model	Continuum Global Hydrological model	Flood hydrographs force hydrodynamic simulations	MATSIRO-GW Global Hydrological Model (GHM)
River routing model	LISFLOOD-Global groundwater and river routing model	Dynrout Extension of PCR-GLOBWB model	Hydraulic flood model (global river routing)	LISFLOOD-FP global river routing model.	CaMa-Flood (version 4.04) model
Flood frequency analysis	Annual maxima discharge; Gumbel distribution estimates discharge for a given return period	Annual maxima flood volumes: Gumbel distribution is fitted for a given return period	Index flood method computes extreme discharge values; regression techniques on geomorphological and climatological variables	A hybrid-clustering approach in conjunction with a flood-index methodology	Annual max water level (0.25-degree grid box) unit catchment; Gumbel distribution estimates peak water level for a given return period
Downscaling method	Spread over "flood points" that are regularly spaced 10 km apart along the 30 arcsec river network	GLOFRIS downscaling module, into high resolution (30 arcsec or ~1 km) hazard maps	No downscaling	No downscaling	Downscaling from 0.25° preserving water volume
Geographical datasets	HydroSHEDS DEM and Drain Direction map	HydroSHEDS derived SRTM30 DEM and river network	A reconditioned SRTM3 (version 4.12) DEM and HydroSHEDS river network	MERIT HydroSHEDS	MERIT-HydroSHEDS
Return Period (years)	Fluvial flood 10, 20, 50, 100, 200, 500, 1000	Fluvial flood 5, 10, 25, 50, 100, 250, 500, 1000	Fluvial flood 25, 50, 100, 200, 500, 1000	Fluvial/Pluvial 5, 10, 20, 25, 50, 75, 100, 200, 250, 500, 1000	Fluvial 5, 10, 20, 25, 50, 100, 200, 250, 500, 1000
Modeled resolution	0.1°	5 arcmin	32 arcsec	3°	0.25°
Output resolution	30 arcsec	30 arcsec	32 arcsec	3 arcsec	arcsec
Reference	https://data.jrc.ec.europa.eu/collection/id-0054	https://www.wri.org/aqueduct	https://www.preventionweb.net/english/hyogo/gar/2015/en/home/data.html	https://www.fathom.global/product/flood-hazard-data-maps/	http://hydro.iis.utokyo.ac.jp/~yamadai/cama-flood/index.html

TABLE 2 | Characteristics of georeferenced global population datasets adapted from Global Partnership for Sustainable Development Data (2023).

	GPWV4	GHSL-Pop	LandScan	WorldPop
Population data	2010 Population and Housing Censuses	GPWv4.10 data	Subnational census and administrative data	GPWv4 census data
Geospatial ancillary inputs	Protected areas and water bodies	Built-up areas mapped in the Global Human Settlement Layer Built Up Extent (GHSL-BUILT)	Roads, land cover, built structures, cities or urban areas, infrastructure, environmental data, protected areas, and water bodies	Roads, land cover, built structures, cities or urban areas, nighttime lights, infrastructure, environmental data, protected areas, and water bodies
Satellite imagery	None	Landsat imagery for 1975, 1990, 2000, 2014	Maxar (formerly DigitalGlobe)	Landsat Enhanced Thematic Mapper (ETM), Landsat, TerraSAR-X, TanDEM-X, DMSP and VIIRS
Source of data adjustment	Official country totals for censuses and UNPD estimates	UNPD estimates	US Census Bureau International Programs estimates	Country-official estimates and UNPD estimations
Method	Areal Weighting	Binary dasymetric mapping	Multi-variable dasymetric	Random forest
Epoch	2000, 2005, 2010, 2015, and 2020	1975, 1990, 2000, and 2015	Annual since 1998	2000–2020
Resolution	30 arcsec (1 km)	250 m, 1 km (World Mollweide) 9 arcsec, 30 arcsec (WGS84)	30 arcsec (1 km)	3 arcsec (100 m)
Data access	https://www.earthdata.nasa.gov/data/projects/gpw	https://human-settlement.emergency.copernicus.eu/ghs_pop2022.php	https://landscan.ornl.gov/	https://www.worldpop.org/

the cascade model structure is provided by Euser et al. (2013) and for the gauged-flow model structure by Sampson et al. (2015). The cascade model structure uses global climate reanalysis data, driving a land surface model to produce flows at locations along a river. The gauged-flow model structure uses gauged-discharge or gauged-precipitation datasets from over 9500 stations as input.

The modeling approaches differ between using regionalization techniques that depend on 180 upstream catchment characteristics (Fathom) and models that need to be complemented by hydrologic simulations (CIMA-UNEP) (Aerts et al. 2020). The gauge models use a growth curve to determine extreme flow that is then input into a hydraulic model that predicts the flood extent and depth for a given return period flow (Trigg et al. 2016). Depending on the GFM model type, the climate model used, or the gauge data used, each GFM will have a different estimated return period extent (Bernhofen et al. 2021).

All the model outputs were converted to a binary flood (depth >0 m), dry (depth $=0$ m) raster for the computations for this study. Exposure analysis was derived by intersecting the flooded areas with spatially distributed exposure datasets for four gridded population products. Summary statistics of inundated areas and population exposure for areas of interest were computed for the Sudd region, South Sudan, and the 10 states.

To evaluate model agreement, we aggregate the wet area extent from the 100-year return period flood extents from all five models to develop categories that indicate how many models agree that an area is flooded. This produces a single dataset with a category as an integer that indicates the number of models that agree.

We conducted this aggregation at the finest resolution across all the models to ascertain consistency and accuracy. A model agreement index (MAI) (Equation 1) is then calculated from these categories for a given region (South Sudan country level and the Sudd region) by summing up the total area of each flooded category, multiplied by the fraction of models that agree in that category, and then dividing this sum by the maximum possible model agreement, resulting in a fraction of model agreement (Trigg et al. 2016)

$$\sum_{i=2}^{N} \frac{i}{N} a_i \quad (1)$$

MAI = Where: A is total flooded area predicted by all models, a_i is the flooded area for an aggregated category, N is the number

TABLE 3 | Comparing modeled flood extent for the Sudd region and South Sudan (SSD) for three different return periods.

Model	Flood return probabilities of 4% and 5%		
GFMs	South Sudan (SSD) flood area extent (km^2)	Sudd region flood area extent (km^2)	Sudd flood area as % of SSD flood area
Aqueduct-4%	78,774	67,783	86
CIMA-UNEP-4%	87,752	68,880	78
Fathom-5%	85,031	65,429	77
JRC-5%	129,772	116,876	90
CaMa-UT-4%	158,629	134,392	85
Model	**Flood return probability of 2%**		
Aqueduct	80,451	69,227	86
CIMA-UNEP	101,546	81,260	80
Fathom	113,027	88,692	78
JRC	139,012	127,805	92
CaMa-UT	165,797	143,838	87
Model	**Flood return probability of 1%**		
Aqueduct	82,158	70,680	86
CIMA-UNEP	104,835	84,059	80
Fathom	132,308	104,829	79
JRC	144,847	129,762	90
CaMa-UT	176,935	153,172	87

of models in comparison, and i is the aggregated category (i.e., number of models in agreement). The index does not assume any single model is more correct than the rest and is solely based on an agreement measure for wet areas only.

3.2 | Satellite Observations of the Sudd Flooding Extent

We employed a satellite remote-sensed method to determine the maximum annual flooding extent in the Sudd study region for 2000–2022. This method uses the Moderate Resolution Imaging Spectrometer (MODIS) land surface temperature (LST) product (MOD11A1). MODIS LST for 2000–2022 was processed using Google Earth Engine. A pixel-based quality control mask was applied to remove pixels impacted by clouds, cloud shadows, high aerosols, and band saturation, and all remaining values were converted to degrees Celsius. All available data were aggregated for each month, and the median was calculated to obtain a complete image that is representative of the full month. Histograms of each monthly image were then created and showed a bi-modal distribution; lower values are assumed to be inundated pixels and higher values are assumed to be dry pixels. The temperature that provided the best split between the distributions (identified by the minimum frequency) was selected as a threshold value for each month that could be used to delineate the flooded and non-flooded areas. The threshold values were applied to create monthly binary flood (inundated or dry) maps as raster flood maps at 0.1° by 0.1-degree grid resolution. MODIS LST has been used to map wetland extents (Ordoyne and Friedl 2008) and rice paddies (Zhang et al. 2017) and can effectively delineate flooded area boundaries during dry, hot periods because inundated areas are often much cooler. MODIS LST data in the Sudd region shows high contrast between the wetland

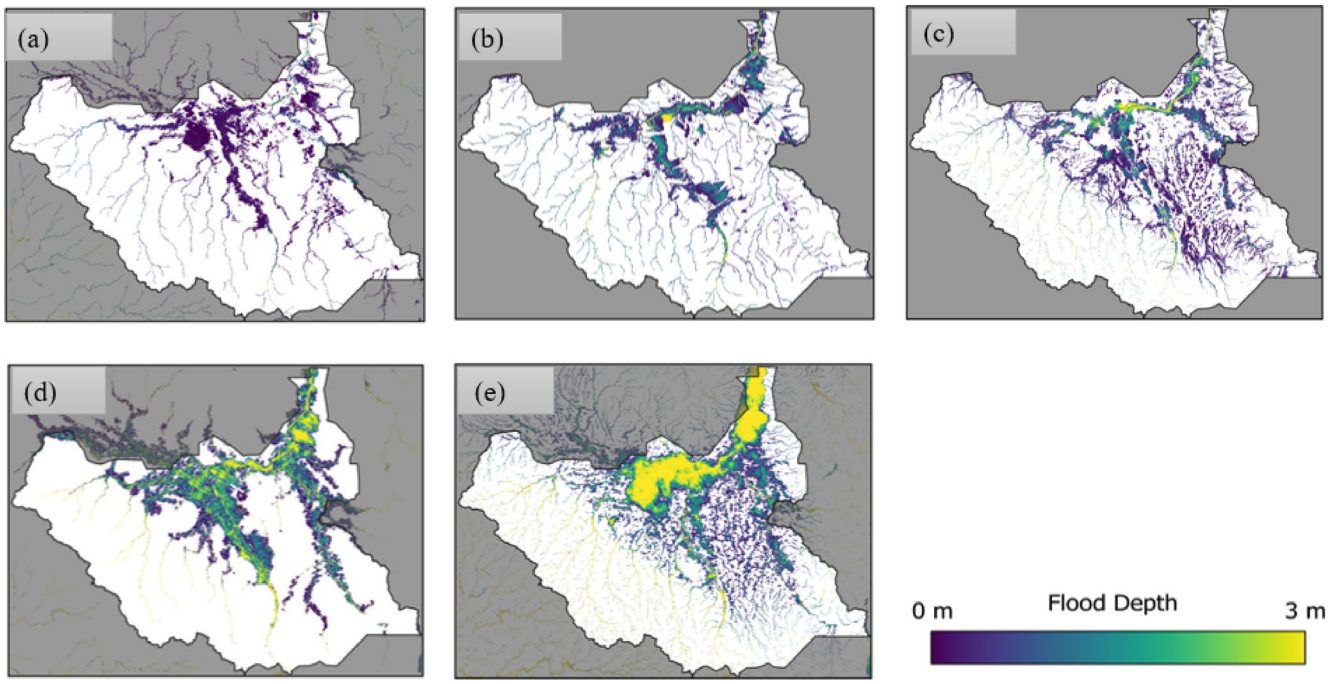

FIGURE 4 | Comparing a 1% probability for flood simulation among 5 GFMs: (a) Aqueduct, (b) CIMA-UNEP/GAR2015, (c) Fathom Global, (d) JRC, and (e) CaMa-UT.

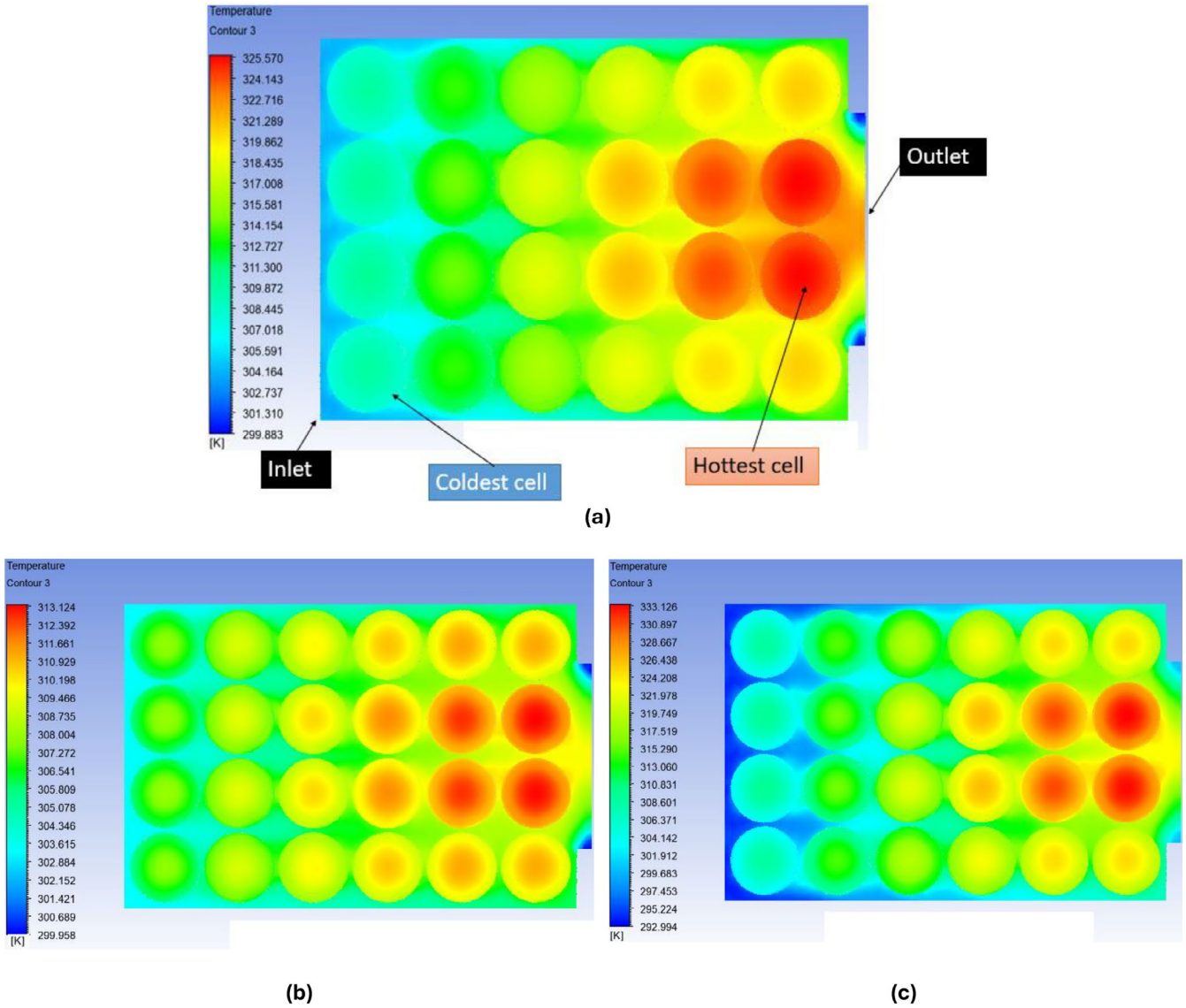

FIGURE 5 | Comparison of detailed area for flood maps among the 5 GFMs: (a) Aqueduct—a 4% probability of flood event, (b) CIMA-UNEP—a 4% probability of flood event, (c) Fathom Global—a 5% probability of flood event, (d) JRC—a 5% probability of flood event, and (e) CaMa-UT—a 4% probability of flood event. Figure (f) is an inset area in the top left of South Sudan map.

area and dry land during the dry season, generally from November to February (Di Vittorio and Georgakakos 2021). Fortunately, the dry season aligns with the period when the Sudd reaches its max extent, thus according to several studies (Sutcliffe and Parks 1999; Rebelo et al. 2012; Di Vittorio and Georgakakos 2018) can be leveraged to delineate the annual maximum flooding extent.

3.3 | Global Gridded Population Data

Given the challenges in estimating the population and households of South Sudan, and for the Sudd region, we make use of global georeferenced population products from open access sources as an alternative approach to estimate South Sudan populations and map spatial distribution. These gridded population products (Table 2) combine census data with remote sensing data to estimate where people live.

All the population datasets were resampled and projected to the same resolution for this study. To ensure consistency among the population products compared, this study only used the most up-to-date epoch for each population dataset and the single most recent year, 2020. The extended data documentation is available through the POPGRID website (https://www.popgrid.org/, last access: June 2023).

Recent works by Smith et al. (2019) and Bernhofen et al. (2021) found that flood exposure estimates are significantly impacted by the population datasets used. The methods for these global population products, their development, and their wide-ranging applications are reviewed in detail by Leyk et al. (2019). In summary, there is not one single product that is systematically more appropriate than the rest.

The GPW approach evenly redistributes source data into target grid cells based on proportions of overlap with no ancillary data

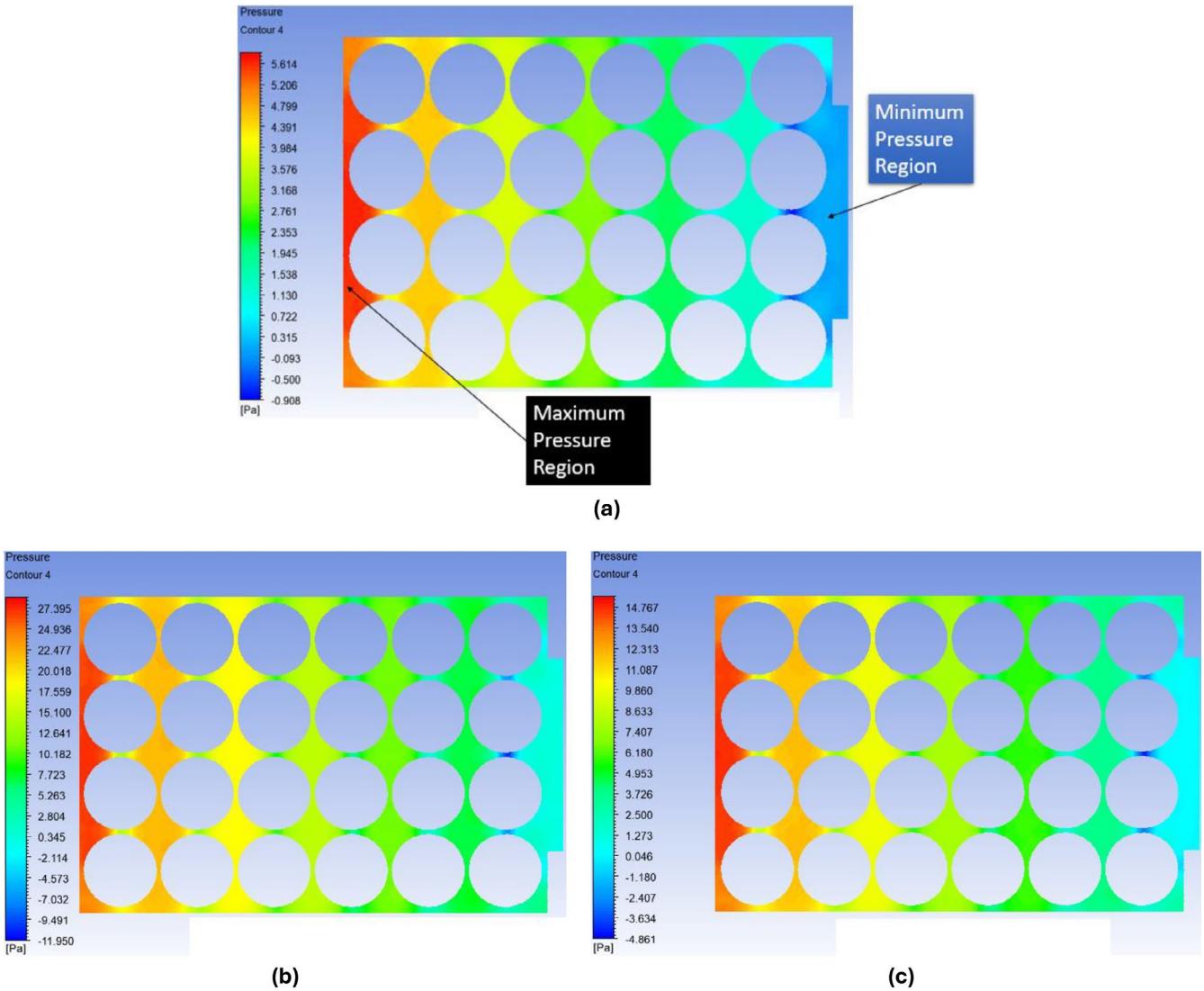

FIGURE 6 | Agreement of the spatial extent for the probability of a 1% flood event among the 5 GFMs: Aqueduct, CIMA-UNEP, Fathom Global, JRC, and CaMa-UT; 0 corresponds to dry area—no model predicting flooding, whilst 1–5 indicate the number of models in agreement.

input informing the process (Goodchild and Lam 1980; Baynes et al. 2022). This assumption (Leyk et al. 2019) is a gross simplification since population distributions are not uniform. The GHSL-Pop approach is grounded on the concept that buildings and their agglomerations (i.e., settlements) are nowadays the main visible and direct manifestation of human presence and activity on the Earth's surface (Leyk et al. 2019; Bernhofen et al. 2021). A limitation associated with GHSL-Pop is its sole use of built-up mapping as detected from satellite imagery, which may miss settlement units that are too small to detect in the rural areas such as the Sudd region.

In comparison, WorldPop and LandScan use similar geospatial ancillary inputs (Table 3), except that the former additionally correlates nighttime light with population distribution. However, nighttime light is sensitive to the level of economic development given some areas such as urban centers and airports exhibit high values despite levels of residential occupancy. A shortcoming of the nighttime light technique is its inability to capture some of the scattered rural settlements and populations in the rural areas around the Sudd and within its islands without electrification. LandScan may perform well in capturing urban population distribution but is less reliable in rural areas (Aubrecht et al. 2016), as satellite imagery may fail to detect certain settlements that are constructed with materials from the grasslands or woody vegetation. WorldPop uses machine learning to identify significant relationships from the input census data and apportions some population to rural areas under the assumption that not all "built-up" areas will be picked up in the satellite imagery. Despite this advantage, among others, the WorldPop model has been criticized for excluding more uninhabited land than do the other datasets due to its clustered populations (Aubrecht et al. 2016).

4 | Results and Discussion

4.1 | Global Flood Hazard Data Agreement

We compared flood hazard extents for different return periods from different global models to represent hazard in the Sudd region. The flood depth was used to compare the range of flood depth across the five different global flood products.

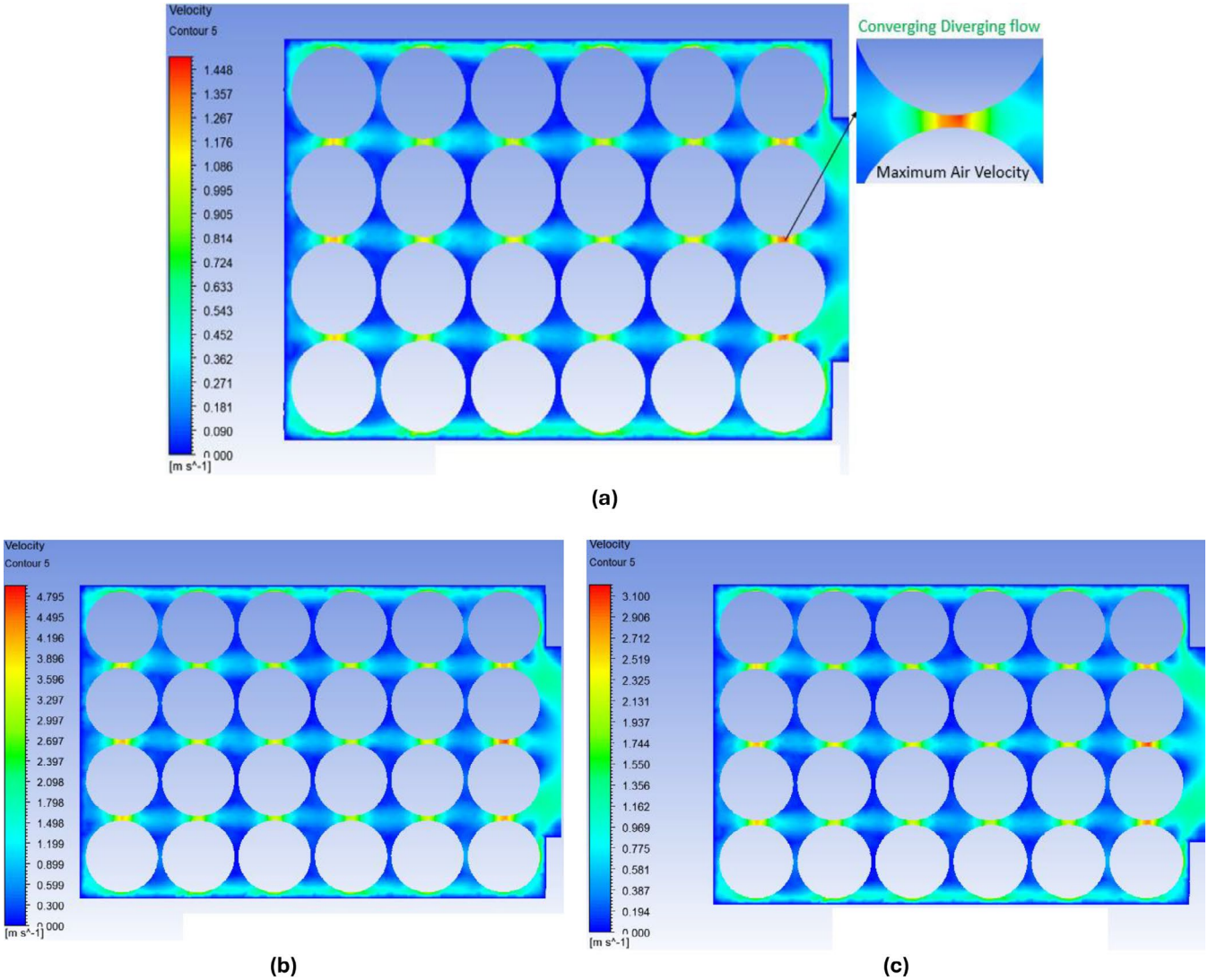

FIGURE 7 | Sudd annual flood extent. The stars on top of the graph correspond to reported flood events (2007, 2008, 2014, 2017, and 2019–22) from Figure 3.

Both CaMa-UT and JRC modeled the largest hazard extent and greater depth of the Sudd flood in a 1% probability of flood event (Figure 4) and in the inset detailed area in a 5% and a 4% probabilities of flood event (Figure 5).

As can be observed, aggregated results (Figure 6) show agreement is higher in the narrow-confined floodplains near the confluences of Bahr el Ghazal, Bahr el Jebel, and Pibor-Baro-Akobo-Sobat systems (dark and bright green colors). Agreement is however least along the peripheral areas of the floodplains and drier areas. Disagreement is also visible in the central area of the Sudd (i.e., between Leer and Bentiu in Unity State, and around the confluence of Sobat and the White Nile in Upper Nile State).

Some disagreement can be attributed to different size rivers that these rivers model. Some models are configured to simulate only major rivers while others incorporate smaller tributaries. For example, Bernhofen et al. (2021) found that in South Sudan the exposure was ~4× more when you consider smaller rivers ($> 50\,km^2$ upstream drainage area) compared to when you only look at major rivers ($> 5000\,km^2$ upstream drainage area).

The differing approaches to global flood hazard mapping result in flood extent disagreement (Aerts et al. 2020; Trigg et al. 2016) and varied performance (Bernhofen et al. 2018), suggesting no single model is uniformly fit for a given purpose. Some of the previous intercomparison studies found large differences between these models in Africa (Trigg et al. 2016) and China (Aerts et al. 2020). An intercomparison study at the country level (Trigg et al. 2016) found high exposure for South Sudan and more agreement between models as all identify the large Sudd wetlands. However, Trigg et al. (2016) also found some disagreement as dynamics of vegetation and evaporation play a dominant role in the Sudd flood extent, and not all models include these processes.

Besides Aqueduct, both the Fathom and CIMA-UNEP that belong to the gauged-flow model structure have a comparably smaller percentage of total flooded areas in the Sudd region (Table 3).

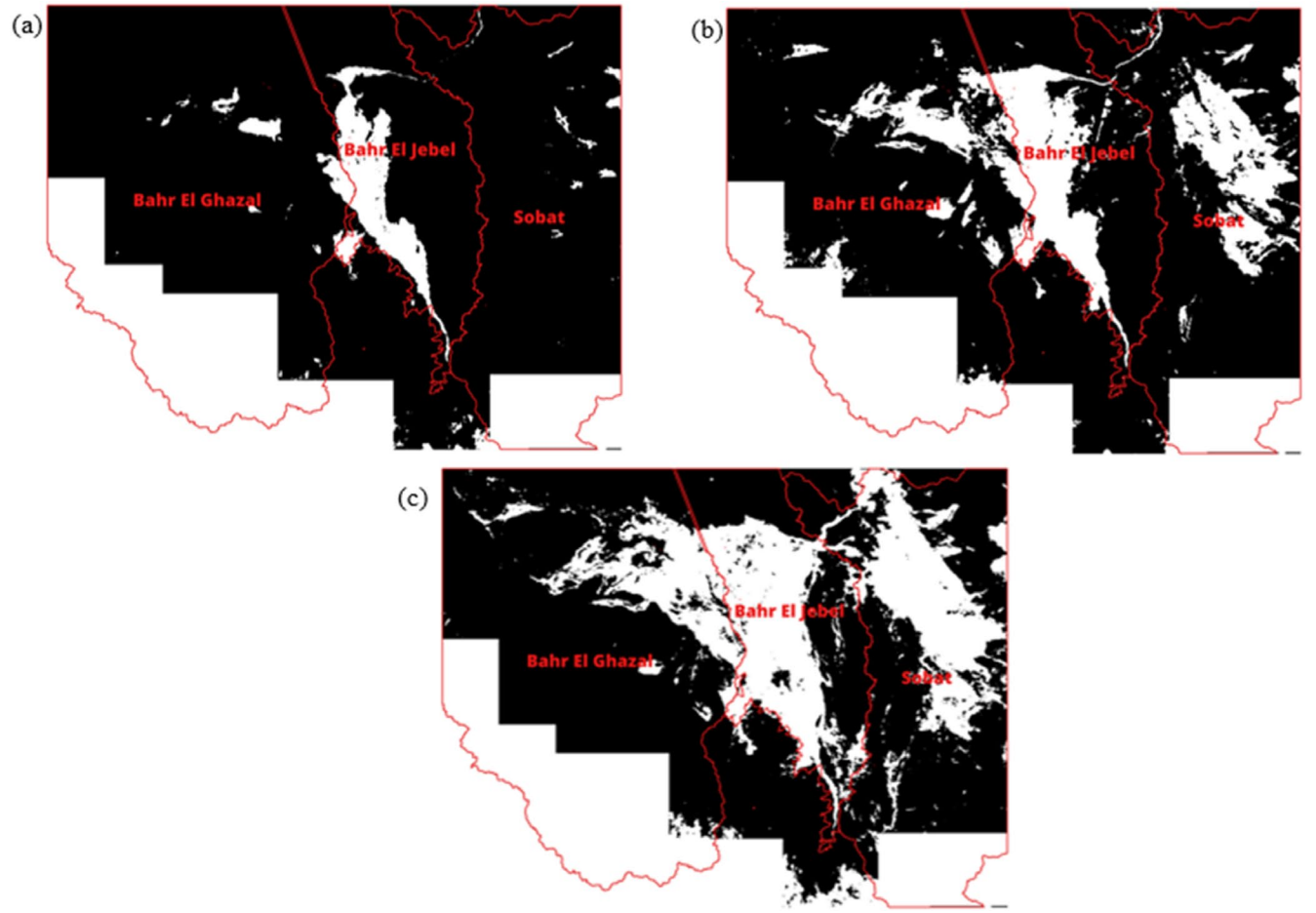

FIGURE 8 | Satellite observation: Sudd annual maximum flood extent: (a) Isolated regime: Representative year 2002 flood extent area (28,000 km^2)—Bahr el Ghazal to the northwest, the Bahr el Jebel to the southcentral, and the Sobat to the extreme northeast are isolated; (b) Connected regime: Representative year 2007 flood extent area (53,000 km^2)—the Bahr el Jebel and Bahr el Ghazal are connected; and (c) Merged regime: Representative year 2022 flood extent area (88,000 km^2)—the Sudd/Bahr el Jebel, the Bahr el Ghazal, and the Sobat are all merged.

The uncertainty associated with the application of the gauged-flow models in the Sudd region could pose some challenges in flood hazard mapping and flood risk management. One such uncertainty, which concerns the estimates of the flooded areas, is that South Sudan gauge stations and data records are limited. The gauges along the Bahr el Jebel/White Nile and the Sudd stopped working during the civil war from 1983 to 2005. There are only about four river gauge stations (Juba, Malakal, Renk, Wau, and Raga) that are operational in the country, but whose readings resumed intermittently only in 2007 after the CPA. The different performances by these gauged-flow models in the Sudd region are probably attributable to the absence or limited availability of gauge stations and historical records of gauge data. Comparably, the underpredicted flood hazards by these two methods could have implications for the utilization of flood exposure results and flood risk management.

4.2 | Satellite Observations of the Sudd Flooding Extent

The maximum annual flood extent estimated for 2000–2022 was produced and is presented in Figure 7.

During the 22 year period, we observe 5 years (2009–2011, 2017, and 2018) with comparatively less annual maximum flooded area, with 2009 exhibiting the least annual extent.

A visual analysis of the 22 Sudd annual maximum flooding extents for this period shows three distinct spatial regimes related to connectivity of the three major wetlands of South Sudan: (1) the Sudd/Bahr el Jebel basin to the central south, (2) the Bahr el Ghazal to the northwest, and (3) the Sobat to the northeast. The three regimes are:

1. Isolated wetlands are shown (Figure 8) with 2002 representing the regime that occurred in 15 years: 2000, 2001, 2002, 2003, 2003, 2004, 2008, 2009, 2010, 2011, 2012, 2013, 2015, 2017, 2018, and 2019.
2. Connected wetlands: the Bahr el Ghazal and the Bahr el Jebel/Sudd connection is continuous in 2005, 2006, 2007, 2014, 2016, and 2019. Figure 8 shows 2007 as the representative maximum flood extent. However, the connectivity of the Sobat, extreme northeast, to the Sudd is not part of this regime.
3. Merged wetlands: in 2020, 2021, and 2022 flood extents from the three basins, the Bahr el Ghazal, the Bahr el

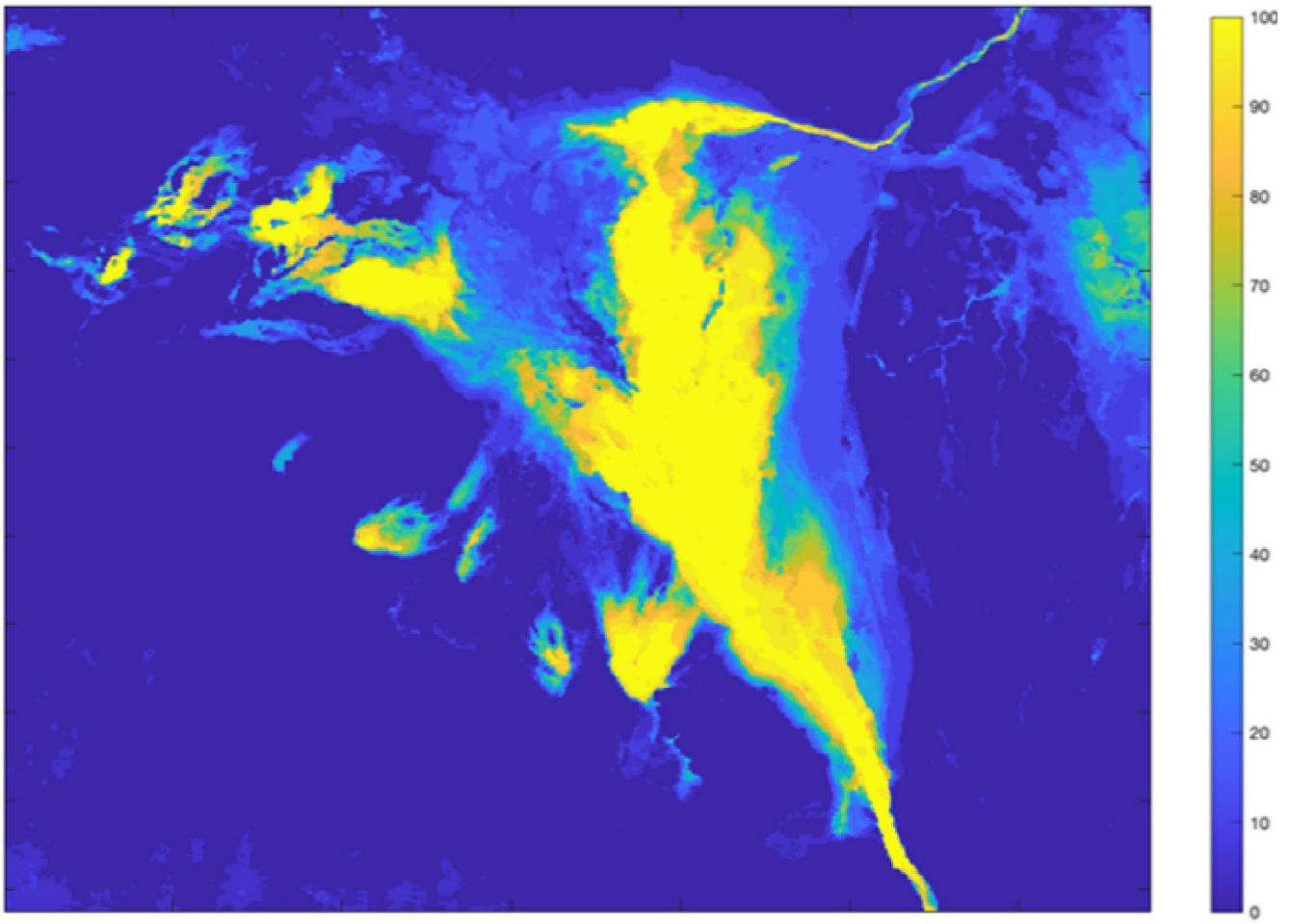

FIGURE 9 | The percentage of years over 22 years that each pixel is flooded. The areas that are flooded in 90%–100% of the annual maximum extent images (yellow) can be considered the Sudd permanent wetlands and major tributaries; the orange area (80%–90%) appears to be a buffer area along the edge of the permanent wetland. The green areas (50%–70%) appears to be the seasonal wetlands that bridge the permanent wetland and the floodplains (30%–40%, light blue).

Jebel/Sudd, and the Sobat are merged. 2022 is representative of this regime illustrated in Figure 8.

In the 22-year period, the Bahr el Jebel, the Bahr el Ghazal, and the Sobat basins appear as separate water bodies until the latest flood years (2021–2022) when they are hydrologically connected by flood water.

The direction of the connecting flow is not clear, even in years (2020–2022) with an apparent continuous connection between the three basins. The Bahr el Ghazal and the Sobat are augmenting flows to the Sudd. This is a point of uncertainty that previous researchers (Sutcliffe and Brown 2018; Sutcliffe and Parks 1999) have identified, but which has not yet been settled. Looking at the far eastern side of the flood maps, we observe a substantial extent of the Sobat basin in some years (2019–2022) that could be amplifying flooding in the Sudd in those years. The Sobat flows may have already filled up the channel capacity at the exit into the white Nile, causing a backwater effect toward the Sudd exit.

The dramatic increase in the flooded area from 2019 to 2022 (Figures 7 and 8) indicates a major change in the Sudd, signaling a whole new flow regime may be taking shape since 2019, with a greater amount of water flowing to the Sudd from the equatorial lakes region, coupled with increased flow from the Bahr el Ghazal and the Sobat basins. The analysis highlights the high spatial and temporal variability of flood extents and flow regimes in the Sudd region. Understanding this complex change and its hydro-ecological implications for the welfare of the populations in the Sudd region is critical for understanding population exposure to flood risks.

We also calculated the likelihood of flooding in the Sudd region. Figure 9 depicts a percentage probability that each pixel is flooded over the 22-year period of satellite observations.

4.2.1 | Comparison of Satellite Observations and GFMs Results

To compare the model projections with the historical observations, we estimated the recurrence interval of the maximum annual flood extent from the 22 years of satellite derived estimates. A statistical analysis was performed, and the 22 annual maxima observations were fitted to the generalized extreme value distribution (GEV). The return intervals from the fitted GEV

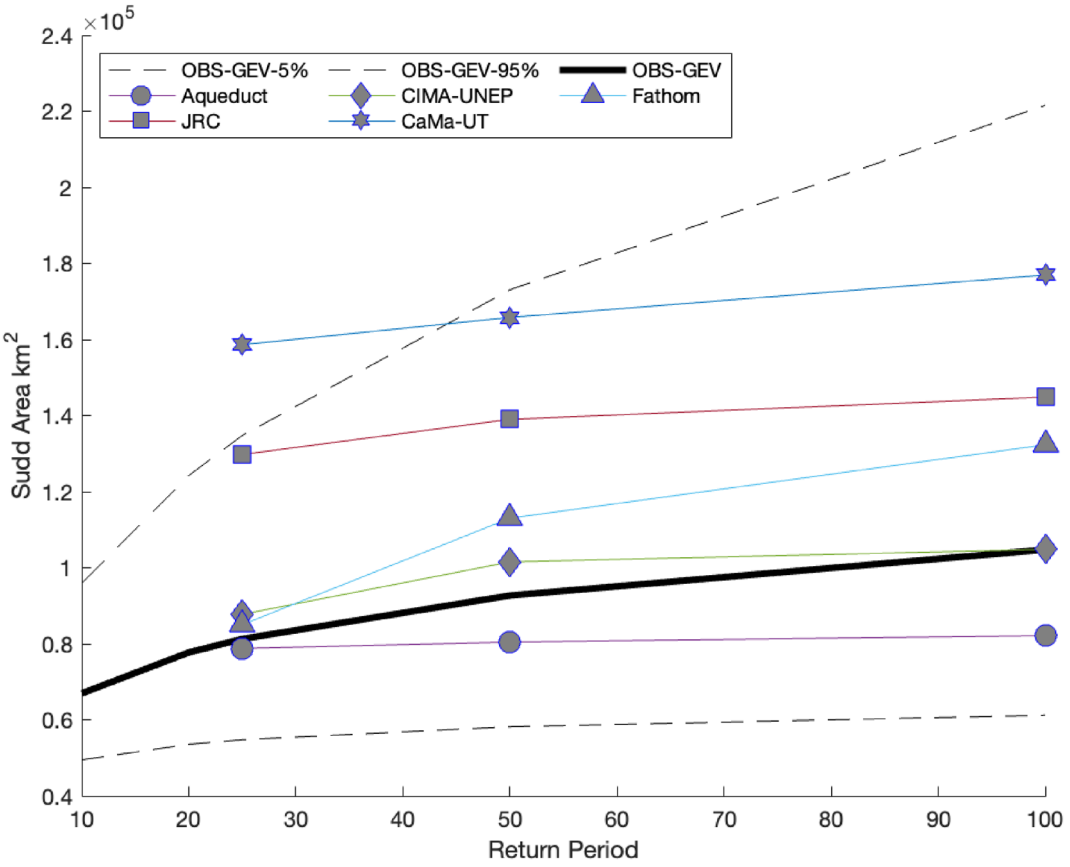

FIGURE 10 | Sudd maximum flood extent: Satellite estimated data and GFMs simulated flood extent across four different return periods.

distribution for the 5–100-year recurrence with 90% uncertainty band is presented in Figure 10.

One goal of this analysis is to identify the GFM that best matched the satellite observation. The measure of model skill is based on the comparison of flood extent for each recurrence interval.

Figure 10 visually compares the frequency curves from the GFM to the Observed GEV median and 5 and 95 confidence limits. Table 5 below presents flooded area root mean square (RMS) error of the maximum annual flood extent between the GFMs projections and the observed GEV estimations for the 5%, 4%, 2%, and 1% floods. Visually and from the Table 4 the CIMA-UNEP model shows the best skill to match the satellite observed flood extent.

The results in Table 4, while quite large, are not unexpected for global models for the Sudd. The Sudd has unique hydrology and hydraulic conditions. All localized modeling efforts such as (Sutcliffe and Parks 1999; Di Vittorio and Georgakakos 2021) have used local data that global models do not have access to and do not do local calibration.

TABLE 4 | Difference of maximum annual flood extent between the GFMs projections and the observed GEV estimations for the 5%, 4%, 2%, and 1% floods.

	Difference from estimated GEV flooded area (estimate from 2000 to 2022) (km^2)		
GFMs	**4%/5%**	**2%**	**1%**
Aqueduct-4%	2501	12,249	22,610
CIMA-UNEP-4%	6477	8846	67
Fathom-5%	3756	20,327	27,540
JRC-5%	48,497	46,312	40,079
CaMa-UT-4%	77,354	73,097	72,167

4.3 | Population Estimates for South Sudan and the Sudd Region

Comparing South Sudan and the Sudd region total population estimates (Table 5), including population density among the five population products, the magnitude of the difference in population estimates was observed. To compare population density, we used South Sudan area, 644,329 km^2, and the Sudd region estimated area, 326,863 km^2, as defined for this study.

The WorldPop-UN adjusted and GHSL-Pop have about the same population estimates for the Sudd region and South Sudan, as both products use the same (UN-adjusted) census data for 2020 as the input data. The GPW estimates about 0.4 million population more than does the LandScan for the Sudd region.

TABLE 5 | Population estimates for South Sudan and the Sudd region.

Population products	South Sudan population	SSD pop density/km^2	Sudd region population	Sudd region pop density/km^2
South Sudan population 2008	8,260,490	13.8	4,577,414	14.0
LandScan Pop 2020	10,543,201	16.4	4,333,702	13.3
World Pop 2020 UN adjusted	11,179,641	17.4	4,370,838	13.4
GHSL-Pop 2020	11,203,766	17.4	5,529,445	17.0
S. Sudan pop projected 2020	13,249,925	20.6	7,334,763	22.4
GPW-Pop 2020	14,206,579	22.0	4,733,662	14.5
World Pop 2020 non-UN adjusted	16,826,744	26.1	6,550,256	20.0

LandScan predicts the least total population for both South Sudan and the Sudd region.

To compare population density for South Sudan and the Sudd region, we used five georeferenced population products (Figure 11).

The LandScan, WorldPop, and GHSL maps show details of the location of settlements in different parts of the country, including clustered population settlement pattern in the Sudd region. There are, however, uncertainties associated with the application of any of these population modeling products. While the gridded population datasets present a static view of population distribution, they fail to account for the dynamics of human migrations that might have occurred between 2008 and 2020. All the products cannot account for migratory populations in the Sudd region as they move seasonally and often residing in less visible shelters that are made of grasses and branches of trees and often located within and under trees. This shortcoming presents challenges in determining dynamic population density and habitations vis-a-vis changing nature of flood risks.

4.3.1 | Population Exposure Calculations

The summary statistics of exposure were calculated first for the Sudd region, then at the South Sudan level. The total exposed and total average population exposed were calculated for each level of analysis at 20, 25, 50, and 100-year return periods using georeferenced population datasets for 2020. Exposure differences calculated for the Sudd region arise when intersecting four different population products with GFMs products across these various simulated food return periods (Figure 12).

The estimated population that is modeled for the Sudd region varies between the global population products used in this study. The Sudd population estimates represent the Sudd region that begins at the entrance of the Sudd in Mongalla, Central Equatoria state and includes part of the Bahr el Ghazal and Sobat systems (Figure 1).

To compare these population estimates, we used the absolute values as modeled by each of the population products, and percentage differences of population exposures, computed by intersecting each population product estimates and simulated flooded area by each of the five GFMs.

The Aqueduct model shows the least exposure for all population data products. The WorldPop product when intersected with Aqueduct shows almost similar percent exposure across the three return periods (Figure 12). GPW estimates the largest population exposures across three return periods: 25-year (2.5 million), 50-year (2.7 million), and 100-year (2.8 million) when intersected with CaMa-UT.

In addition to the differences in absolute values of the flooded extent area, we assessed percentage differences (Figure 12) of population exposures. Comparing percentage differences of population exposures between population products captures how each product distributes population density in the Sudd region vis-à-vis GFMs' delineation of the wetland extent.

All the population products intersected with both JRC and CaMa-UT show high percent exposure to flood risks. The GPW estimate produces the largest population exposure, 54% using the JRC model and 61% using the CaMa-UT model for a 1% probability of flood occurrence.

The differences in methods each population product uses to estimate the population and the variations in the estimated flooded area extent attributed to the algorithm configurations of each GFM are reflected in the differences in population exposures for the Sudd.

5 | Conclusion

This study analyzes and compares global flood models and intersects the results with gridded population products to quantify population exposure to flood hazard in the Sudd region. Findings from this study are relevant beyond South Sudan and demonstrate the global significance of using multiple sources for flood mapping and population estimates, rather than relying on one global flood model and one population estimate. The results indicate that 0.8–2.8 million people are currently exposed to the 100-year return period flood extent, depending

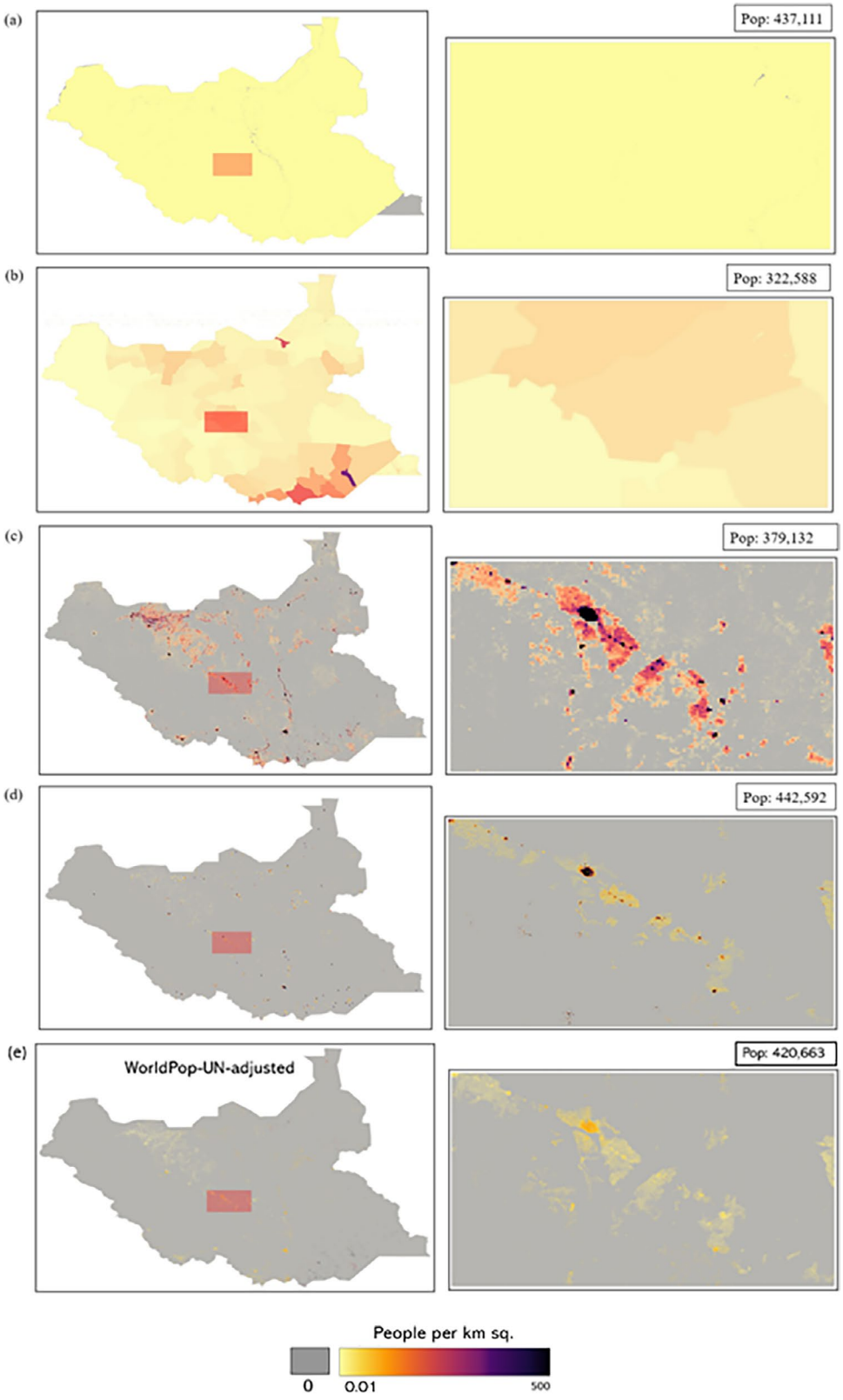

FIGURE 11 | Comparison of population density products: The left column represents the population density map of South Sudan—(a) WorldPop—non-UN-adjusted, (b) GPW, (c) LandScan Global, (d) GHSL-Pop, and (e) WorldPop—UN-adjusted with the inset area; and the right column indicates the population density detailed area—the number of people in the inset area for each product is indicated in the corresponding text boxes.

on the flood model and population dataset used. The uncertainty in this estimate is attributable to variation within flood extent estimates and geospatial population estimates.

Aggregated results of the model agreement intercomparison indicate all five global models agree on key flood-prone areas within and around the Sudd permanent boundary and in the

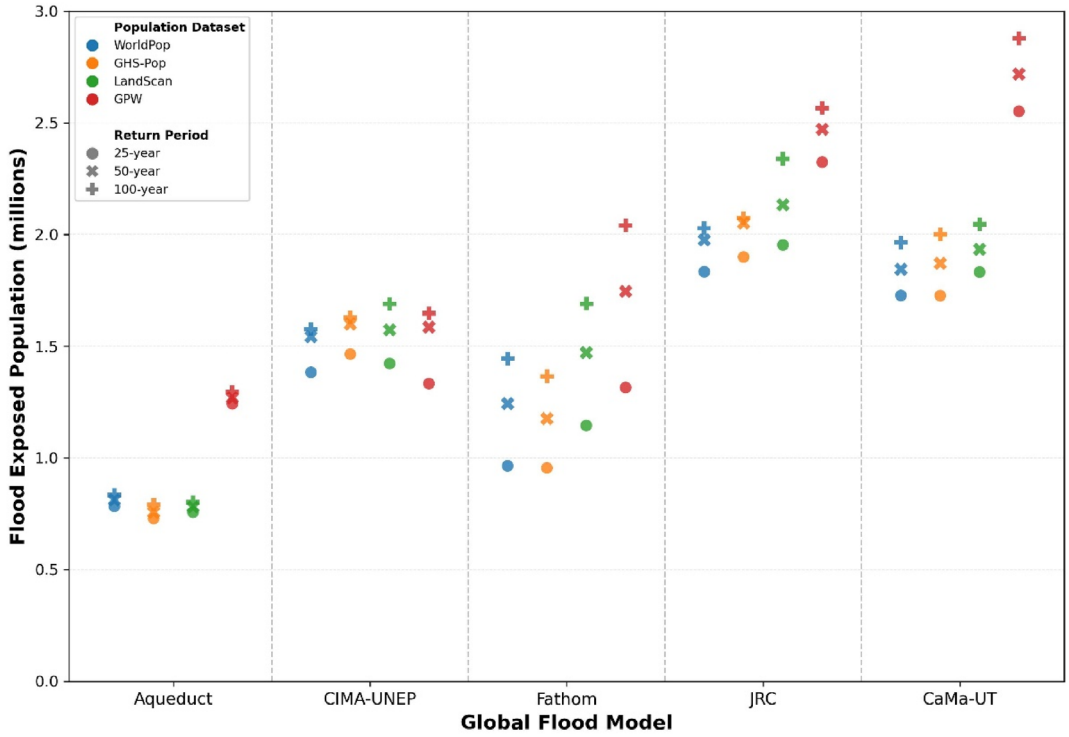

FIGURE 12 | Population exposure for the Sudd region: Intersecting GFMs and gridded population products.

confined and restricted floodplains, consistent with the effects of seasonal floods that spill over the banks of the Sudd Nile and inundate the adjacent surrounding areas. The aggregated GFM analysis indicates agreement is higher around the permanent wetland, and along the seasonal wetlands, tributaries, and channels.

Comparison of the global flood modeling with satellite flood observations reveals the limitations of both data sources. However, there is a considerable agreement between modeled flood hazards and satellite—derived flood extents in areas and locations that are prone to seasonal flooding in the Sudd region. The synthesis of the MODIS derived Sudd flood extents indicates a different regime from 2019 to 2022, characterized by increasing intensity and frequency of flood event. The new regime flood extent results in consequential impacts on the population exposed to flood risks as they impede society's wellbeing and economic development progress.

Intercomparison of the population density among the four population products demonstrates that WorldPop and GHSL-Pop population distributions favor patterns of rural, traditional community settlements that are typically in the form of clusters of villages that are located along the tributaries of the Sudd Nile and within the floodplains. However, the georeferenced population products are static as they fail to capture unique dynamics of the population mobility in the Sudd region, which is characterized by rapid change in local population, incomplete census, and lack of long-term or time series dataset.

This study therefore recommends future studies on the modeling of the dynamics of adaptative behaviors, including migration in response to flood risks to inform sustainable management of flood disasters in the Sudd region.

Despite the variation in results between models in the remote rural villages in the Sudd floodplains, this inter-model-comparison is an important step toward a better understanding of modeling flood hazard, which is urgently needed for both current risk and climate change projections in places such as South Sudan with poor data infrastructure and where fluvial flood risk is still unmapped. These findings provide hitherto unavailable insights into flood exposure in South Sudan, to inform flood management decisions and disaster reduction responses in the Sudd region. They also provide an example of how global datasets can underpin policy and decision-making in Africa and other data scarce regions.

Acknowledgments

This article is an output from the REACH Programme, funded by UK Aid from the UK Foreign, Commonwealth and Development Office (FCDO) for the benefit of developing countries (Project Code 201880). However, the views expressed and information contained in it are not necessarily those of or endorsed by FCDO, which can accept no responsibility for such views or information or for any reliance placed on them.

Funding

The authors have nothing to report.

Conflicts of Interest

The authors declare no conflicts of interest.

Data Availability Statement

The data that support the findings of this study are available in European Commission Joint Research Centre at https://data.jrc.ec.europa.eu/collection/id-0054. These data were derived from the following resources available in the public domain: Joint Research Centre (JRC), https://data.jrc.ec.europa.eu/collection/id-0054—GloFRIS Aqueduct, https://www.wri.

org/aqueduct—CIMA-UNEPGAR 2015, https://www.preventionweb.net/english/hyogo/gar/2015/en/home/data.html—Gridded Population of the World (GPW), https://www.earthdata.nasa.gov/data/projects/gpw—Global Human Settlement Layer (GHSL), https://human-settlement.emergency.copernicus.eu/ghs_pop2022.php—LandScan Global, https://landscan.ornl.gov/—World Pop, https://www.worldpop.org/.

References

Aerts, J. P. M., S. Uhlemann-Elmer, D. Eilander, and P. J. Ward. 2020. "Comparison of Estimates of Global Flood Models for Flood Hazard and Exposed Gross Domestic Product: A China Case Study." *Natural Hazards and Earth System Sciences* 20, no. 12: 3245–3260. https://doi.org/10.5194/nhess-20-3245-2020.

Andreadis, K. M., O. E. J. Wing, E. Colven, C. J. Gleason, P. D. Bates, and C. M. Brown. 2022. "Urbanizing the Floodplain: Global Changes of Imperviousness in Flood-Prone Areas." *Environmental Research Letters* 17, no. 10: 104024. https://doi.org/10.1088/1748-9326/ac9197.

Aubrecht, C., R. Gunasekera, J. Ungar, and O. Ishizawa. 2016. "Consistent Yet Adaptive Global Geospatial Identification of Urban–Rural Patterns: The IURBAN Model." *Remote Sensing of Environment* 187: 230–240. https://doi.org/10.1016/j.rse.2016.10.031.

Balek, J. 1977. *Hydrology and Water Resources of Tropical Africa*. Vol. 8, Developments in Water Science Series. Elsevier.

Baynes, J., A. Neale, and T. Hultgren. 2022. "Improving Intelligent Dasymetric Mapping Population Density Estimates at 30 m Resolution for the Conterminous United States by Excluding Uninhabited Areas." *Earth System Science Data* 14, no. 6: 2833–2849. https://doi.org/10.5194/essd-14-2833-2022.

Bernhofen, M. V., S. Cooper, M. A. Trigg, et al. 2022. "The Role of Global Datasets for Flood Risk Management at National Scales." https://doi.org/10.1002/essoar.10508948.1.

Bernhofen, M. V., M. A. Trigg, P. A. Sleigh, C. C. Sampson, and A. M. Smith. 2021. "Global Flood Exposure From Different Sized Rivers." *Natural Hazards and Earth System Sciences* 21, no. 9: 2829–2847. https://doi.org/10.5194/nhess-21-2829-2021.

Bernhofen, M. V., C. Whyman, M. A. Trigg, et al. 2018. "A First Collective Validation of Global Fluvial Flood Models for Major Floods in Nigeria and Mozambique." *Environmental Research Letters* 13, no. 10: 104007. https://doi.org/10.1088/1748-9326/aae014.

Birkett, C., R. Murtugudde, and T. Allan. 1999. "Indian Ocean Climate Event Brings Floods to East Africa's Lakes and the Sudd Marsh." *Geophysical Research Letters* 26, no. 8: 1031–1034. https://doi.org/10.1029/1999GL900165.

Borgomeo, E., C. Chase, N. Salazar Godoy, and V. Osei Kwadwo. 2023. *Rising From the Depths Water Security and Fragility in South Sudan*. World Bank.

Di Vittorio, A. V., and K. P. Georgakakos. 2021. "Hydrologic Modeling of the Sudd Wetland using Satellite-based Data." *Journal of Hydrology: Regional Studies* 37: 1–13.

Di Vittorio, C. A., and A. P. Georgakakos. 2018. "Land Cover Classification and Wetland Inundation Mapping Using MODIS." *Remote Sensing of Environment* 204: 1–17. https://doi.org/10.1016/j.rse.2017.11.001.

Egypt Nile Control Dept (Ministry of Water Resources and Irrigation). 1933. *Nile Historical Discharge*. Government Press.

Euser, T., H. Winsemius, S. Hrachowitz, H. H. G. Savenije, and M. Hrachowitz. 2013. "A Framework to Assess the Realism of Model Structures Using Hydrological Signatures." *Hydrology and Earth System Sciences* 17, no. 5: 1893–1912.

Evans-Pritchard, E. E. 1940. *The Nuer: A Description of the Modes of Livelihood and Political Institutions of a Nilotic People*. Oxford University Press.

Global Partnership for Sustainable Development Data. 2023. "POPGRID Data Collaborative." Last access: June 2023.

Goodchild, M. F., and N. S. Lam. 1980. "Areal Interpolation: A Variant of the Traditional Spatial Problem." *Geo-Processing* 1, no. 3: 297–312.

Gowdy, J., and H. Lang. 2016. *The Economic, Cultural and Ecosystem Values of the Sudd Wetland in South Sudan: An Evolutionary Approach to Environment and Development*. UNEP/The Evolution Institute.

Hirabayashi, Y., M. Tanoue, O. Sasaki, X. Zhou, and D. Yamazaki. 2021. "Global Exposure to Flooding From the New CMIP6 Climate Model Projections." *Scientific Reports* 11, no. 1: 3740. https://doi.org/10.1038/s41598-021-83279-w.

Howell, P., M. Lock, and S. Cobb, eds. 1988. *The Jonglei Canal: Impact and Opportunity*. Cambridge University Press.

Howell, P. P. 1983. "The Impact of the Jonglei Canal in The Sudan." *Geographical Journal* 149: 286–300.

Hurst, H. E., and P. Phillips. 1938. "The Nile Basin." In *The Hydrology of the Lake Plateau and Bahr El Jebel*, vol. 5. Government Press.

Internal displacement Monitoring Centre. 2023. *Global Report on Internal Displacement*. Humanitarian Hub Office.

Johnson, D. H. 1992. "Reconstructing a History of Local Floods in the Upper Nile Region of the Sudan." *International Journal of African Historical Studies* 25, no. 3: 607.

Johnson, D. H. 2019. "Adaptation to Floods in the Jonglei Area of The Sudan: An Historical Analysis." In *The Ecology of Survival: Case Studies From Northeast African History*, 173–192. Taylor and Francis.

Jongman, B., P. J. Ward, and J. C. J. H. Aerts. 2012. "Global Exposure to River and Coastal Flooding: Long Term Trends and Changes." *Global Environmental Change* 22, no. 4: 823–835. https://doi.org/10.1016/j.gloenvcha.2012.07.004.

Lake Victoria Basin Commission. 2020. "Lake Victoria Rising Water Levels."

Lamberts, E. 2009. *The Effects of Jonglei Canal Operation Scenarios on the Sudd Swamps in Southern Sudan*. Master's thesis. University of Twente.

Leyk, S., A. E. Gaughan, S. B. Adamo, et al. 2019. "The Spatial Allocation of Population: A Review of Large-Scale Gridded Population Data Products and Their Fitness for Use." *Earth System Science Data* 11, no. 3: 1385–1409. https://doi.org/10.5194/essd-11-1385-2019.

Mahgoub Mohamed, T. 2021. "Forecasting of Monthly Flow for the White Nile River (South Sudan)." *American Journal of Water Science and Engineering* 7, no. 3: 103. https://doi.org/10.11648/j.ajwse.20210703.12.

Mason, I. M., C. G. Harris, G. Picton, and J. M. Moore. 1992. "Monitoring Wetland Hydrology by Remote Sensing: A Case Study of the Sudd Using Infrared Imagery and Radar Altimetry." Proceedings of the Central Symposium of the 'International Space Year' Conference.

McMichael, C., S. Dasgupta, S. Ayeb-Karlsson, and I. Kelman. 2020. "A Review of Estimating Population Exposure to Sea-Level Rise and the Relevance for Migration." *Environmental Research Letters* 15, no. 12: 123005.

Mohamed, Y. A., W. G. M. Bastiaanssen, and H. H. G. Savenije. 2004. "Spatial Variability of Evaporation and Moisture Storage in the Swamps of the Upper Nile Studied by Remote Sensing Techniques." *Journal of Hydrology* 289: 145–164.

Mohamed, Y., and H. H. G. Savenije. 2014. "Impact of Climate Variability on the Hydrology of the Sudd Wetland: Signals Derived From Long Term (1900-2000) Water Balance Computations." *Wetlands Ecology and Management* 22, no. 2: 191–198. https://doi.org/10.1007/s11273-014-9337-7.

Mohamed, Y. A., B. J. J. M. Van den Hurk, H. H. G. Savenije, and W. G. M. Bastiaanssen. 2005. "Impact of the Sudd Wetland on the Nile Hydroclimatology." *Water Resources Research* 41, no. 8.

Nicholson, S. E. 2017. "Climate and Climatic Variability of Rainfall Over Eastern Africa." *Reviews of Geophysics* 55, no. 3: 590–635. https://doi.org/10.1002/2016RG000544.

Nicholson, S. E., and X. Yin. 2001. "Rainfall Conditions in Equatorial East Africa During the Nineteenth Century as Inferred From the Record of Lake Victoria." *Climatic Change* 48, no. 2–3: 387–398. https://doi.org/10.1023/A:1010736008362.

Nile Basin Intiative (NBI). 2020. "NBI Technical Reports: Wetlands and Biodiversity Series." Sudd Wetland Monograph - Volume 1 : Overview of the Sudd Wetland Ecosystems and Land use.

Ordoyne, C., and M. A. Friedl. 2008. "Using MODIS Data to Characterize Seasonal Inundation Patterns in the Florida Everglades." *Remote Sensing of Environment* 112, no. 11: 4107–4119. https://doi.org/10.1016/j.rse.2007.08.027.

Parks, A. 2024. "The World's Largest Land Mammal Migration Confirmed in South Sudan." *African Parks. Retrieved. December, 2025*.

Persico, G., W. M. Seyoum, and E. W. Peterson. 2024. "Interrelationships Between NDVI, Surface Water, and Regional Hydro-Climatic Variables In the Sudd Wetland." *Wetlands* 44, no. 7: 92.

Rebelo, L. M., G. B. Senay, and M. P. McCartney. 2012. "Flood Pulsing in the Sudd Wetland: Analysis of Seasonal Variations in Inundation and Evaporation in South Sudan." *Earth Interactions* 16, no. 1: 1–19. https://doi.org/10.1175/2011EI382.1.

Rentschler, J., P. Avner, M. Marconcini, et al. 2023. "Global Evidence of Rapid Urban Growth in Flood Zones Since 1985." *Nature* 622, no. 7981: 87–92. https://doi.org/10.1038/s41586-023-06468-9.

Rentschler, J., M. Salhab, and B. A. Jafino. 2022. "Flood Exposure and Poverty in 188 Countries." *Nature Communications* 13, no. 1: 3527. https://doi.org/10.1038/s41467-022-30727-4.

Sampson, C. C., A. M. Smith, P. D. Bates, et al. 2015. "A High-Resolution Global Flood Hazard Model." *Water Resources Research* 51, no. 9: 7358–7381.

Smith, A., C. C. Sampson, J. P. Savage, P. D. Bates, J. Neal, and G. Robert Brakenridge. 2019. "New Estimates of Flood Exposure in Developing Countries Using High-Resolution Population Data." *Nature Communications* 10, no. 1: 1814.

Sosnowski, A., E. Ghoneim, J. J. Burke, E. Hines, and J. Halls. 2016. "Remote Regions, Remote Data: A Spatial Investigation of Precipitation, Dynamic Land Covers, and Conflict in the Sudd Wetland of South Sudan." *Applied Geography* 69: 51–64. https://doi.org/10.1016/j.apgeog.2016.02.007.

Sutcliffe, J., and E. Brown. 2018. "Water Losses From the Sudd." *Hydrological Sciences Journal* 63, no. 4: 527–541. https://doi.org/10.1080/02626667.2018.1438612.

Sutcliffe, J. V., and Y. P. Parks. 1999. "Water." In *The Hydrology of the Nile*. International Water Management Institute.

Tootchi, A., A. Jost, and A. Ducharne. 2019. "Multi-Source Global Wetland Maps Combining Surface Water Imagery and Groundwater Constraints." *Earth System Science Data* 11, no. 1: 189–220. https://doi.org/10.5194/essd-11-189-2019.

Travaglia, C., J. Kapetsky, and G. Righini. 1995. *Monitoring Wetlands for Fisheries by NOAA AVHRR LAC Thermal Data*. FAO/SDRN.

Trigg, M. A., C. E. Birch, J. C. Neal, et al. 2016. "The Credibility Challenge for Global Fluvial Flood Risk Analysis." *Environmental Research Letters* 11, no. 9: 094014. https://doi.org/10.1088/1748-9326/11/9/094014.

UNEP (United Nations Environment Programme). 2018. *South Sudan: First State of Environment and Outlook Report*. UNEP.

UNESCO World Heritage Centre Ramsar Convention Secretariat. 2006. "The Sudd Wetland (Site No. 1607) Designation. Ramsar Sites Information Service."

UNESCO World Heritage Centre. Ministry of Culture, Youth, and Sports. 2017. "Sudd Wetland." South Sudan.

United Nations. 2023. "Wetlands for Our Common Future." World Wetlands Day, 2 February.

Yamazaki, D., D. Ikeshima, J. C. Neal, et al. 2017. "MERIT DEM: A New High-Accuracy Global Digital Elevation Model and Its Merit to Global Hydrodynamic Modeling." *AGU Fall Meeting Abstracts*, Vol. 2017, H12C-04.

Zhang, G., X. Xiao, C. M. Biradar, et al. 2017. "Spatiotemporal Patterns of Paddy Rice Croplands in China and India From 2000 to 2015." *Science of the Total Environment* 579: 82–92. https://doi.org/10.1016/j.scitotenv.2016.10.223.

Supporting Information

Additional supporting information can be found online in the Supporting Information section. **Data S1:** jfr370168-sup-0001-Supinfo.docx.